Article

The International Journal of
Robotics Research
2015, Vol. 34(9) 1195–1210

DOI: 10.1177/0278364915583880
ijr.sagepub.com

Grasp planning to maximize task coverage

Yun Lin and Yu Sun

Abstract

This paper proposes a task-oriented grasp quality metric based on distribution of task disturbance, which could be used to search for a grasp that covers the most significant part of the disturbance distribution. Rather than using a uniformly distributed task wrench space, this paper models a manipulation task with a non-parametric statistical distribution model built from the disturbance data captured during the task demonstrations. The grasp resulting from maximizing the proposed grasp quality criterion is prone to increasing the coverage of most frequent disturbances. To reduce the computational complexity of the search in a high-dimensional robotic hand configuration space, as well as to avoid the correspondence problem, the candidate grasps are computed from a reduced configuration space that is confined by a set of given thumb placements and thumb directions. The proposed approach has been tested both in simulation and on a real robotic system. In simulation, the approach was validated with a Barrett hand and a Shadow hand in several manipulation tasks. Experiments on a physical robotic platform verified the consistency between the proposed grasp metric and the success rate.

Keywords

Task-oriented grasping, task modeling, task disturbance distribution, grasp quality measure

1. Introduction

In robotics, grasping has been an active research area that involves many important research topics. Among them, the grasp synthesis problem has attracted significant attention. To solve this problem, numerous approaches and algorithms have been developed. A detailed review of various approaches can be found in Sahbani et al. (2012). One direction of the grasp synthesis research is grasp planning that applies optimization theory to search for contact placement on an object and the optimal posture of the hand, which gives rise to the difficulty in choosing a quality criterion for the optimization procedure. In the literature, the existing grasp quality measures can be associated to either contact locations or hand configuration. Both have been studied thoroughly. A detailed discussion of several grasp quality measures within the two groups was provided by Suárez et al. (2006). In this paper, we present a novel grasp quality measure that utilizes contact locations.

When a grasp is modeled with contact between the object and the fingers, one considers that the contact should provide a firm grasp under external disturbances. A widely used quality criterion in this group is the force-closure property that measures the capability of a grasp to withstand external disturbance wrenches from any direction (Kirkpatrick et al., 1992). Related research was developed by Ferrari and Canny (1992), Pollard (1994), Miller et al. (2003), and Hsiao et al. (2011), who proposed grasp-planning approaches to find force-closure grasps. The force-closure quality measure is task-independent, in which evenly distributed wrenches in all directions were assumed (Bicchi and Kumar, 2000).

For many manipulation tasks, however, such as writing and handling a screwdriver, a task-related grasp criterion can be applied in order to choose grasps that are most appropriate to meeting specific task requirements. A manipulation task refers to "the process of moving or rearranging objects in the environment" (Brock et al., 2008), so the force and motion requirements are basic task descriptions that commonly exist in every task (Lin et al., 2012). In terms of the force requirement, the object to be manipulated would interact with the environment, and the interactive wrench on the object would be a disturbance to the grasp. Therefore, a task-oriented grasp should be efficient

Department of Computer Science and Engineering, University of South Florida, FL, USA

Corresponding author:
Yu Sun, Department of Computer Science and Engineering, University of South Florida, 4202 E Fowler Avenue, ENB 118, Tampa, FL 33620, USA.
Email: yusun@cse.usf.edu

in resisting the disturbance wrenches required for a task. One typical task-oriented grasp method is to choose a suitable task wrench space (TWS) and then measure how well it can be fitted into a grasp wrench space (GWS) (Borst et al., 2004; Han et al., 2000; Haschke et al., 2005; Li and Sastry, 1988; Pollard, 1994). Few works have considered the task information in grasp planning due to the difficulty of modeling a task (Borst et al., 2004; Li and Sastry, 1988; Sahbani et al., 2012). To obtain the TWS in reality, sensors are necessary to measure the contact regions and contact normals in human demonstration, which remains a challenge. This is the main reason why most works empirically approximate the TWS rather than actually measure it. Instead of a wrench space ball used in a force-closure quality measure, Li and Sastry (1988) used a six-dimensional wrench space ellipsoid to better approximate a task to facilitate the computation of the quality measure. The research by Haschke et al. (2005) approximated the TWS as a task polytope. Kruger and van der Stappen (2011, 2013) and Kruger et al. (2012) developed algorithms to generate two or three feasible contact locations given one single wrench and wrenches in its neighborhood. However, their works were not generalized to most of the manipulation tasks where multiple interactive wrenches may occur.

Pollard (1994) proposed the object wrench space (OWS), which takes the complete object geometry into consideration. The OWS integrates all disturbance wrenches that can be exerted anywhere on the object. Borst et al. (2004) presented an algorithm to approximate the OWS by an ellipsoid and to measure how well the OWS ellipsoid can be fitted into a GWS. The idea of OWS takes all possible disturbances into account, which is good for unknown tasks but is not task-specific; for a specific task, a grasp does not need to perform the whole OWS but only the required TWS, which should be a subset of the whole OWS.

Another difficulty of task-oriented grasp planning is the computational complexity of searching in a high-dimensional hand configuration space. It is, therefore, natural to introduce human experience to constrain the search space (Billard et al., 2008; Hueser and Zhang, 2008; Romero et al., 2008). Aleotti and Caselli (2010) used data gloves to map human hand to robotic hand workspace and captured TWS in virtual reality. They also considered a database of candidate grasps, and grasps were evaluated by a task-related quality measure. However, the correspondence problem has been a crucial issue to map between two different configuration spaces of the human hand and the robotic hand. Research in Pollard (2004) searched for candidate grasps by a shape-matching algorithm and evaluated the grasps by a task-oriented criterion. However, the TWS was also modeled by experience rather than actually measured from the demonstrated task.

This paper expands our previous work (Lin and Sun, 2013b) to address the task-oriented grasp-planning problem. The main contributions of the paper are the following:

1. The task property was measured from real human demonstration data, other than estimated or approximated by experience. Human demonstration was carried out in a virtual reality environment. The users interacted with the environment via a haptic device Phantom OMNI (Section 2.2) and received haptic feedback when they controlled the virtual object to interact with the environment. The task-related disturbance from the environment to the object was captured during the task execution.
2. The task requirement is modeled based on the distribution of the task disturbance (Section 2.2). Rather than simple pick-and-place tasks that have been investigated thoroughly in the literature, we move to interactive tasks that are full of uncertainties. Instead of considering only the shape of the TWS, the proposed approach takes into account the task disturbance distribution measured from human demonstration, since it is possible that disturbance wrenches occur more frequently in some areas than others. The resulting grasp should be efficient in balancing disturbances that frequently occur.
3. A novel task-oriented grasp quality metric is proposed, called the task coverage grasp quality metric (Section 2.4). A real-life robotic hand has limited grasping force that is usually determined by the power of its actuators. For many interactive tasks, it is impossible to guarantee a firm grasp that can resist all possible disturbances, especially spikes that rarely happen. We aim to find a grasp that best allocates the capability of the robotic hand to cover the main disturbances of the task, instead of the rare cases. To move on from pick-and-place tasks, and move into interactive tasks that are full of uncertainties, we proposed this new measure to estimate how likely it is that a grasp will be maintained during an interactive task. To reduce the computational complexity of the search in the high-dimensional robotic hand configuration space, we utilized our previous grasp-planning approach presented in Lin and Sun (2014), which integrates human strategy (thumb placement and direction, as well as grasp type) into grasp planning (Section 2.6). The proposed approach has been tested both in simulation and on a real robotic system, as described in Section 3.

2. Grasp analysis

2.1. Grasp preliminaries

Considering a multi-fingered robotic hand grasping an object, a grasp comprises n contact points. The contact can be modeled by three types: point contact without friction, hard finger, and soft finger (Murray et al., 1994). Here, we consider only the hard finger model, that is, point contact with friction (PCWF), which is widely used in grasp analysis because it has no difficulty in generalizing the model.

Using Coulomb's friction model, the contact force $f_i \in \Re^3$ has the following constraint:

$$\mathcal{F}_i = \left\{ f_i | \frac{1}{\mu_i^2}({f_{it1}}^2 + {f_{it2}}^2) < f_{i\perp}^2 \right\} \quad (1)$$

where f_{it1} and f_{it2} are two tangential force components, $f_{i\perp}$ is the normal force component, and μ is the coefficient of friction. With a given friction coefficient, the maximum tangential force is determined by the normal force. Thus, each contact force f_i is constrained to a friction cone. The friction has a vertex at the contact point, and the axis is along the contact normal, with an opening angle of $2\tan^{-1}\mu$.

For the convenience of computation, the circular friction cone is usually linearized and approximated with an m-sided pyramid. Then, any contact force f_i that is within the constraint of the friction cone can be represented as a convex combination of the m force vectors on the boundary of the cone:

$$f_i \approx \sum_{j=1}^{m} \alpha_j f_{ij} \quad (2)$$

where coefficient $\alpha_j \geq 0$, and $\sum_{j=1}^{m} \alpha_j \leq 1$. If the boundary force vector f_{ij} is assumed to be of unit magnitude along the normal component, then the normal magnitude of the contact force f_i is bounded to be 1, that is, $||f_{i\perp}|| \leq 1$. Each local contact force will generate a force and torque in the object coordinate, grouped as an object wrench $w_i \in \Re^6$. Then, the net resultant wrench can be transformed from the local contact forces through the grasp matrix

$$w = Gf \quad (3)$$

where $f = [f_1^{\mathrm{T}}, \ldots, f_n^{\mathrm{T}}]^{\mathrm{T}}$ is a vector concatenating all contact forces, and $G = [G_1, \ldots, G_n] \in \Re^{6 \times 3n}$ is the grasp matrix. GWS is defined as the set of all possible resultant wrenches w that can be generated by all feasible contact forces lying within the friction cone. GWS is the convex hull of all the object wrenches. The magnitude of object wrenches scales linearly with the contact forces that are limited by the joint capabilities. For comparison, the upper bound is typically set to be 1. Ferrari and Canny (1992) defined the unit GWS by bounding unitary L_1 or L_∞ norm of the normal contact force. Since the contact force is under the frictional constraint, constraint on the normal component also imposes an upper bound on the contact force. Here, by imposing the upper bound of the L1 norm to be 1, the set of all possible resultant object wrenches produced by the grasp is defined as unit GWS (UGWS):

$$UGWS = \{Gf | f_i \in \mathcal{F}_i, ||f_{i\perp}|| \leq 1\} \quad (4)$$

An important grasp property is force closure. A grasp is force closure if for any wrench w there exists a solution $f \in \mathcal{F}$. In other words, a force-closure grasp is able to equilibrate external force and moment in any direction without violating the friction constraints. It is equivalent to the condition that there exist strict internal forces f_{in}, such that $Gf_{in} = 0$. Thus, if the origin of the wrench space is included in the interior of GWS, then the grasp is force closure. Similar to the GWS, a task can also be described as the space of disturbance wrenches from the environment that the object must resist. Ferrari and Canny (1992) quantified the force-closure property by the magnitude of disturbance wrench that can be compensated for by the grasp in the worst case. If no task-oriented information is provided to form a subset of the whole space of wrenches, a typical TWS is a six-dimensional ball T_{ball} centered at the wrench space origin, where external disturbance is uniformly weighted (left in Figure 1). The grasp quality is the reciprocal of the scale to enlarge the UGWS so that it contains the whole TWS:

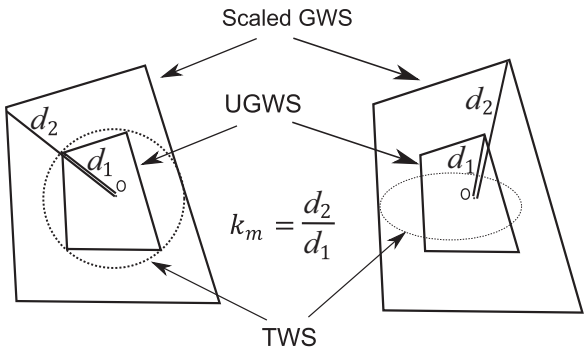

Fig. 1. Grasp quality measures for (left) task ball represented by the dashed circle, and (right) task ellipsoid represented by the dashed ellipse; k_m is the linear scale factor to enlarge UGWS so that it encloses the entire TWS.

$$Q_m(G) = \frac{1}{k_m} \quad (5)$$

$$k_m(G) = min(k) | T_{ball} \subset k \cdot UGWS \quad (6)$$

where $k_m(G)$ is the minimum magnitude of normal contact force in order to resist all task wrenches. The larger k_m is, the greater the effort needed for a grasp to balance the task wrench along the weakest direction. Grasp planning is to find the maximum $Q(G)$, the reciprocal of $k_m(G)$.

2.2. Measure of task wrench

Instead of using a uniform ball, the quality measure in equation (5) can also be used for different task requirements, such as a TWS approximated by a task ellipsoid or a polytope.

Most of the existing work (Haschke et al., 2005; Li and Sastry, 1988; Pollard, 2004) relied on experience to estimate TWS and predict the contact disturbance. For example, to

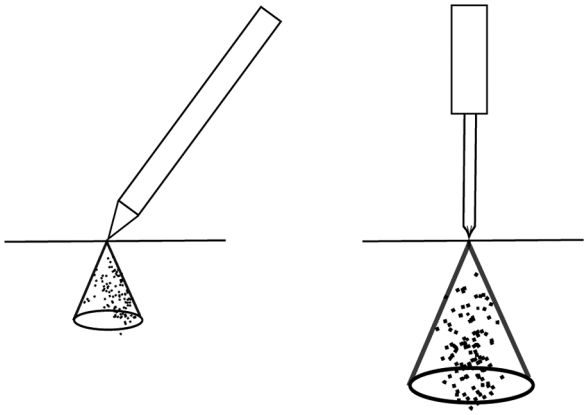

Fig. 2. Disturbance distribution of two tasks. Left: a writing task with a pen; right: a screwing task with a screwdriver.

manipulate such tools as a pen, screwdriver, scoop, fork, toothbrush, and so on, the contact disturbance is expected to be applied to the tips of those tools. Then, the empirical task-oriented disturbance wrench space is a friction cone applied to the tip.

Moreover, the task is considered only by the shape of the GWS without taking the wrench distribution into account, where the wrenches are assumed to be uniformly distributed in the space. However, this is rarely the case. Compare a writing task and the manipulation of a screwdriver, for example. Although both require the grasp to resist disturbance force applied to the tip, they have different disturbance distributions, as illustrated in Figure 2. For the writing task, the main disturbance wrench is the force pointed in the upper-left direction and the torque generated along with the force. Hence, the GWS should be able to apply the opposite force to resist the disturbance, which is distributed primarily in the right area of the friction cone shown in the figure. The main disturbance wrench of the screwdriver is the normal force to the surface and the rotational torque, which is generated by the physical constraint from the screw head, around the principal axis of the screwdriver. In the figure, we only show the force subspace for comparison purposes. Also, the expected disturbance force of the screwdriver is larger than that of the pen. As a result, different distributions of wrenches in a TWS would prefer different grasps.

Therefore, we propose to characterize the TWS and represent the task wrench distribution in it with a task wrench cluster (TWC). It is not trivial to capture the task wrenches applied on physical objects, and collect enough wrenches to form a cluster that could represent the task wrench distribution well. Therefore, we implemented a simulation environment that has a virtual reality environment for visual feedback and a six-dimensional haptic device Phantom Omni for interaction control and haptic feedback. The Phantom Omni allows users to control a virtual object in terms of three-dimensional position and three-dimensional orientation and provides them with three-dimensional haptic feedback of the interaction force between the haptic interaction point (HIP) and the virtual environment. Although a single device cannot control a multi-link body or soft objects, the HIP can be a representation of a rigid body composing the majority of daily tools.

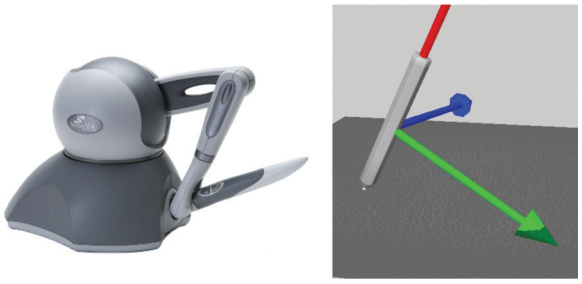

Fig. 3. A user interface for demonstration. Left: the haptic device, Phantom Omni; right: virtual environment.

The virtual reality environment was developed based on Chai3D (http://www.chai3d.org), an open-source C++ library for computing haptic feedback, visualization, and interactive real-time simulation. It integrates Open Dynamic Engine (ODE) for collision detection and dynamics simulation and OpenGL library for graphical visualization. For each task, a user was asked to manipulate a virtual tool using the haptic device (see Figure 3 for example). The three-dimensional collision forces of the tool with the environment were captured every iteration, with a sampling rate of 100 Hz, and three-dimensional torques are computed from the collision forces. All wrenches (forces and torques) collected during the task form a TWC for that particular task:

$$TWC = \{w(i) \in \Re^6 | w(i) = w_c(i) + w_n(i)\} \qquad (7)$$

where $w(i)$ is a wrench at the ith iteration, $w_c(i)$ is the wrench generated by the contacts between the tool and the environment, and $w_n(i)$ is a non-contact wrench.

The non-contact wrench $w_n(i)$ is an offset wrench that includes forces not acting on the surface of the object, such as gravity and the inertial force. Gravity is the force acting on the center of mass on the object along the vertical direction with zero torque. The direction of gravity relative to the object coordinate frame changes with the motion of the object, so the task of rotating an object is to stabilize a set of gravities along multiple directions.

2.3. Study on disturbance distribution

In this section, the simulated disturbance distribution is verified and the distribution model is studied.

2.3.1. Verification on simulated disturbance data. Since the proposed grasp planning relies heavily on simulated disturbance measure, it is necessary to validate how reliable and realistic the simulated data is. Thus, we evaluated the

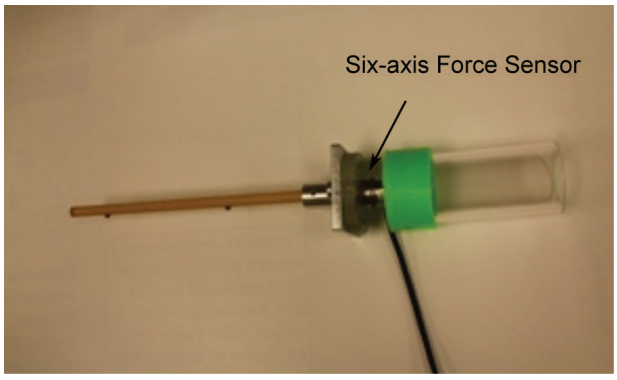

Fig. 4. Tool designed to verify disturbance obtained in simulation. This tool has a force sensor, a handle, and a stick.

simulated data by comparing it with real measurements on a physical tool. To measure the real data, we designed a physical tool, as shown in Figure 4, which is incorporated with a six-axis Nano17 force sensor connecting a handle and a stick. The object wrenches can be measured by the force sensor. This tool can mimic a long-shaped tool that has a handle. The same manipulation tasks can be demonstrated both in simulation and using the physical tool, and the task wrenches were captured in both environments.

We used this tool to execute some interactive tasks with a plane. The actions being tested included sliding and rotational motions, which produce supportive force, frictional force, and rotational torques on the object. The same model of the tool was used in simulation. The distributions from the measured wrenches by the sensor were compared with the wrench distributions obtained in simulation. Each task presented similar distributions. Only the rotational manipulation is shown as an example in Figure 5. Figure 5(a) and (b) shows the disturbance forces in simulation and on the physical tool. To compare the distributions, quantile–quantile (Q–Q) plots were used to plot the relationship between the two sets of data, simulation and reality, as given in Figure 5(c) to (e). A Q–Q plot is a widely used probability plot that is utilized to determine if two data sets have a common distribution by plotting their quantiles against each other (Wilk and Gnanadesikan, 1968).

A Q–Q plot is an excellent graphical method to compare the shapes of distributions and provide a graphical view of how their distribution properties such as location, scale, and skewness are similar or different. In such a plot, points are formed from the quantiles of the data. If the resulting points roughly follow a straight line with a positive slope, the two distributions being compared are similar or linearly related. If the line is diagonal, the two distributions are the same. It can be observed that the points in this study lie roughly on a straight line except for a few outliers, indicating that the distributions of simulation are close to the real measurement. The position and slope of the line indicate the relative shift in location and scale of the samples, which is reasonable, because the samples are measured in different coordinate systems, and the sample scale in simulation can be adjusted by the parameters of the haptic generation model. Therefore, it was verified that the simulation could be used to characterize the wrench distribution of those tasks involving rotational and sliding interactions, though we were unable to verify the complete performance of the simulator for every possible interaction.

2.3.2. Study of the distribution model. To study the distribution of the disturbance, we compared the distribution data with a standard uniform distribution and a normal distribution by a Q–Q plot. Figure 6 shows Q–Q plots of sample data against a standard uniform distribution and a normal distribution for the two aforementioned example tasks. According to the Q–Q plots versus a uniform distribution shown in the left column of the figure, both task disturbance distributions are distinct from a uniform distribution, so the task disturbance is not evenly distributed. The distributions of task disturbance are not close to a normal distribution either (Figure 6(b) and (d)), since none of them lie roughly on a line. Therefore, the distribution model of a task disturbance cannot be characterized as a uniform distribution or a normal distribution.

Because the probability distribution model of disturbance is unknown and the shapes of Q–Q plots change with tasks, we built a non-parametric statistical distribution of the disturbance from the TWC measured by demonstration for each task. Then, to reduce the computational complexity, a smaller set of data points could be randomly down-sampled based on the non-parametric statistical distribution.

2.4. Quality measure based on distribution of task disturbance

The quality measure k_m in equation (5) measures the minimum scale of UGWS in order to enclose the entire TWS, which quantifies an absolute constraint in the worst case where the robot should not drop the object. This grasp metric is reasonable when considering only the shape of the TWS, but it does not take into account the distribution of wrench samples in the space. Consider the scenario of two different GWS for the same TWC in a TWS shown in Figure 7(a) and (b), respectively. The TWS have wrench samples distributed mainly in the left area and some scattered in the right area. The two UGWS have the same shape but differ in their locations. Grasp 1 has a higher ability to apply wrenches in the left area, while grasp 2 has a higher ability to apply wrenches in the right area. If measured by k_m, there is no difference between the two grasps considering only the shape of the TWS, as they require the same minimum effort in order to balance all task wrenches. However, with a relatively small value of scale $k < k_m$, grasp 1 captures the majority of wrench samples in TWC. It implies that, compared to grasp 2, grasp 1 requires less effort to resist the frequently occurring wrenches, thereby resulting in higher efficiency of the power consumption.

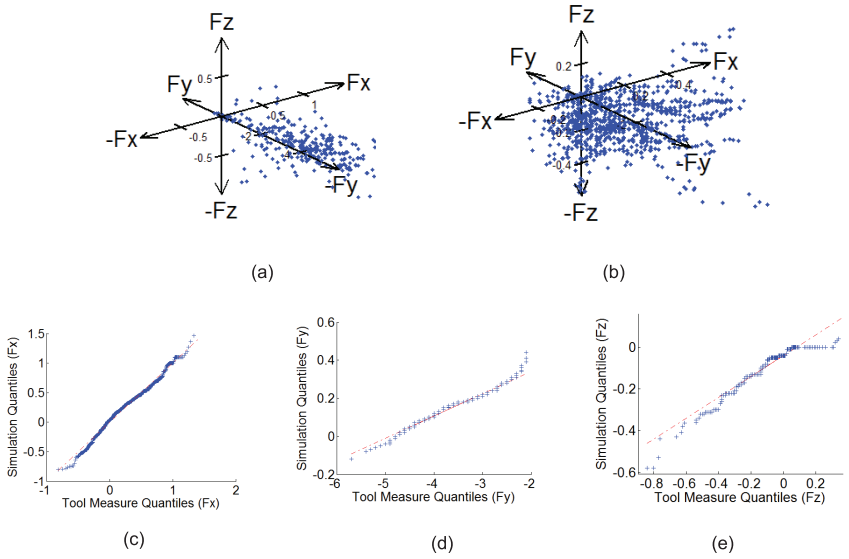

Fig. 5. Example disturbance force of manipulating a screwdriver measured in simulation, the physical tool, and robot wrist in robot execution. (a) Disturbance force measured in simulation; (b) disturbance force measured from tool sensor; (c) to (e) Q–Q plot of distribution of F_x, F_y and F_z in simulation against real tool measure.

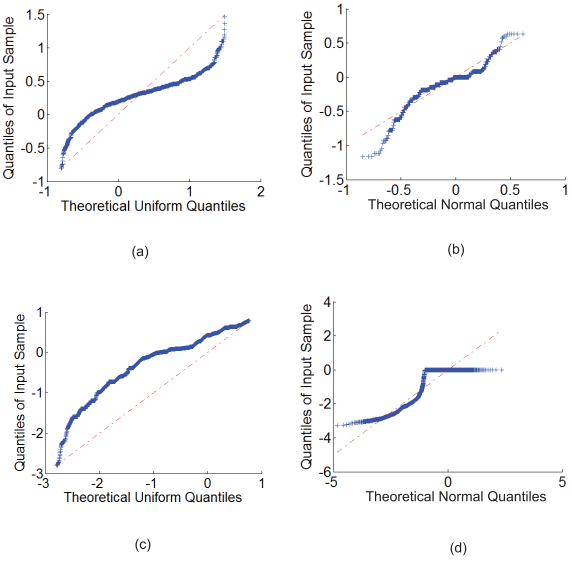

Fig. 6. Q–Q plots to compare sample disturbance data with two standard distribution models. Top row: Q–Q plots for a screwdriver task; bottom row: Q–Q plots for manipulating a knife; left column: Q–Q plots of sample data versus uniform distribution; right column: Q–Q plots of sample data versus normal distribution.

In cases where a robotic hand is not capable of covering all the TWC without exceeding some force limit, it makes more sense to capture as much of the TWC as possible.

2.4.1. The proposed grasp quality measure. Intuitively, the grasp quality can be defined as the ratio of TWC that can be covered by the GWS that is linearly scaling with UGWS by a factor of k (the magnitude of normal contact force, which is an indicator of the robotic finger capability). We define $W(G)$ as the subset of all wrenches in TWC, which are within the scaled GWS for a given k:

$$W(G) = \{\forall w(i) \in TWC | w(i) \in GWS\} \tag{8}$$

The grasp quality can be represented as

$$Q(G) = \frac{|W(G)|}{|TWC|} \tag{9}$$

where $|W(G)|$ is the cardinality of the set $W(G)$, that is, the number of the task wrench samples covered by the GWS, and $|TWC|$ is the cardinality of the set TWC, that is, the number of all wrenches in the TWC. Obviously, $0 \leq Q(G) \leq 1$. The physical meaning of quality measure $Q(G)$ is, given a capability constraint k on the normal contact forces, the percentage of task wrenches that can be resisted by the grasp. With this new grasp quality measure, we will be able to find an optimal grasp G that maximizes $Q(G)$, so it is able to apply the required task wrenches as many as possible, without exceeding a certain amount of contact force.

2.4.2. Selecting k. In some scenarios, the selection of k, the scale factor to determine the size of GWS from UGWS, will affect the selection of grasp, since as k increases, Q increases nonlinearly. Here, we illustrate the influence of k with two grasps in three different scenarios. Since the two grasps may have distinct UGWS, the two UGWS would require different scale factors, k_{m1} and k_{m2}, to cover the

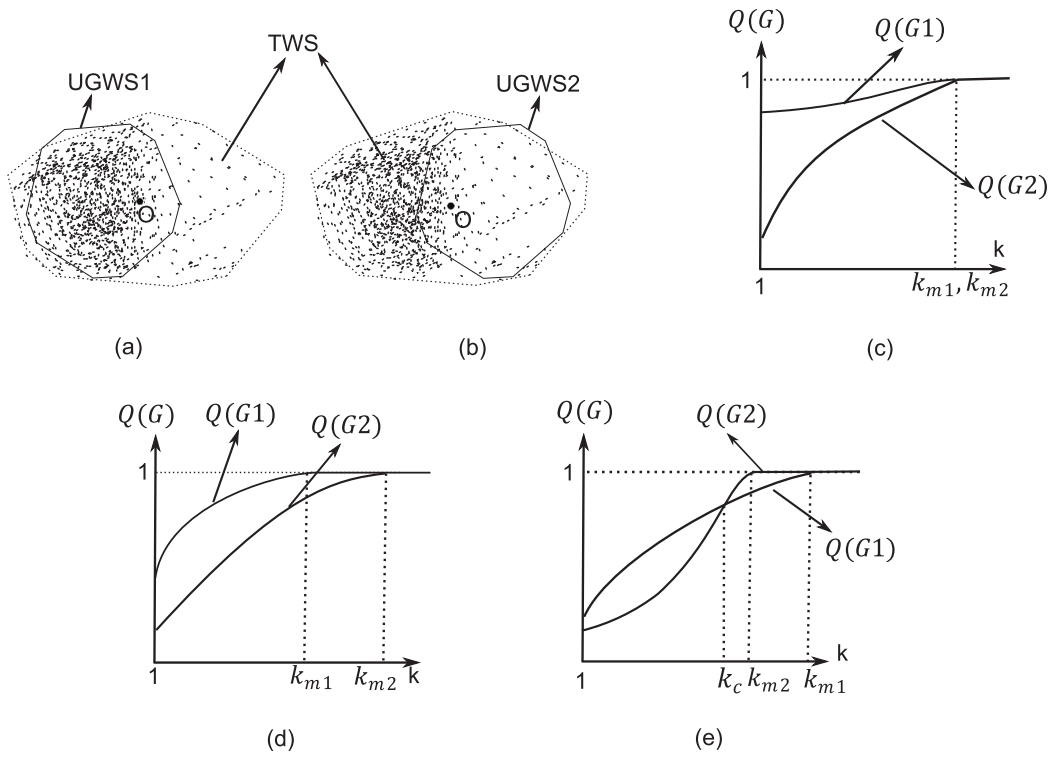

Fig. 7. Comparison of quality measure Q in different scenarios. (a), (b): Two GWS, given the same TWS; (c) to (e): compare the plots of $Q(G1)$ and $Q(G2)$ as a function of scale k in three cases. (c) Scenario 1: the quality plots of the two grasps intersect at $k_{m1} = k_{m2}$, so for all $k < k_m$, $Q(G1) > Q(G2)$. Thus, if measured by $Q(G)$, grasp 1 is better than grasp 2, but they have the same quality if measured by the existing quality metric k_m. (d) Scenario 2: the two grasp plots intersect at k_{m2}, and $k_{m2} > k_{m1}$. For all $k < k_{m2}$, $Q(G1) > Q(G2)$. Thus, the result of our proposed quality measure agrees with the existing quality measure k_m. (e) Scenario 3: the two grasp plots intersect at some $k < k_m$, and the comparison of $Q(G)$ between the two grasps differs depending on the choice of k.

entire TWC. In scenario 1, shown in Figure 7(c), where $k_{m1} = k_{m2}$ and for all $k < k_{m1,m2}$, $Q(G1) > Q(G2)$, selecting grasp 1 is always better than or equal to selecting grasp 2. In scenario 2, shown in Figure 7(d), where $k_{m2} > k_{m1}$, and for all $k < k_{m2}$, $Q(G1) > Q(G2)$, selecting grasp 1 is always better than or equal to selecting grasp 2. However, in scenario 3, shown in Figure 7(e), the two grasp quality plots intersect at some random $k_c < k_{m1,m2}$, so $Q(G1) > Q(G2)$ when $k < k_c$, and it is the opposite when $k > k_c$. Then, selecting grasp 1 or grasp 2 depends on the selection of k. Therefore, it is important to choose a meaningful and reasonable k.

Since scale k stands for the amount of normal contact force the robotic hand is expected to apply, we suggested a scale k_0 by considering both the capability of the robotic hand and the task requirement. This paper provides an example of k_0 selection that considers both the robotic hand capability and the features of the TWC.

In our validation experiments, we also used this k_0 selection scheme as a consistent rule for comparisons. Let $a(i) = \|f(i)\|$, which is the magnitude of $f(i)$, the force component in a given TWC; then, $max(a(i))$ represents the maximum magnitude of all contact forces in TWC. Further, k_0 is determined by the smaller value between the $max(a(i))$ and the maximum force f_{max} that can be applied by the robotic hand, considering the capability of robot actuators, written as

$$k_0 = min(max(a(i)), f_{max}) \tag{10}$$

for all $i = 1,\ldots,T$, where T is the number of wrench samples in the TWC. Because the shape of the GWS does not usually fit with the shape of the TWC well, when k_0 is selected by $max(a(i))$, GWS does not always cover all the wrenches in the TWC.

In this paper, we used a Barrett hand for the experiment in a real environment. The maximum finger force of the Barrett hand is 20 N, so we set $f_{max} = 20$ in order to bound k_0; k_0 can also be set to other empirical values, for example the amount of force that humans usually apply in a manipulation. Further, k_0 can also simply be the hand capability constraint on the contact force, so a grasp will be generated to best allocate the capability of the robotic hand to resist most disturbances in the task. For fragile objects, k_0 can be a smaller value to impose a strict limit on normal contact force, so that the resulting grasp will not break the object but can still hold the object with small contact forces.

2.5. Computational efficiency of grasp quality

To compute the quality of a grasp, GWS is computed as the convex hull of all the possible wrenches that could be generated at all the contact points, and then all samples of the TWS must be checked to determine if they are inside

the scaled GWS. Convex hull is computed by a quick hull algorithm using the Qhull C++ library, where the average case complexity is considered to be $O(mnlog(mn))$ (Barber et al., 1996), where n is the number of contact points, and m is the number of vectors used to approximate the friction cone.

To check if a point is inside the scaled GWS, one can test if the query point lies in the inward area of each facet of the convex hull. Comparing the point with one facet of the convex hull takes constant time. Thus, comparing a point with all facets of the convex hull is the worst case, taking $O(K)$ time, where K is the number of facets of the convex hull. To check if all samples are inside the convex hull takes $O(KL)$ time, where L is the number of task sampling points from the distribution of the disturbance.

2.6. Incorporation of thumb placement constraint into grasp planning

Grasp planning can be treated as an optimization problem, which searches for the maximum value of the high-dimensional quality function Q (e.g. force-closure property). The quality measure is determined by contact points of the hand on the object, and contact points are further determined by the hand posture as well as the relative wrist positions and orientations. Therefore, Q is a function of hand posture and position:

$$Q = f(p, w) \tag{11}$$

where $p \in R^D$ is the hand posture and $w \in R^6$ is the position and orientation vector of the wrist. The dimensionality D depends on the degrees of freedom (DOFs) of the robotic hand and p is the vector that contains the robotic hand's joint angles.

Since a number of anthropomorphic hands have a high number of DOFs to be as powerful as a human hand, thus introducing complexity to the search in the optimization, much work has focused on providing constraints to the search space to reduce the computational complexity of the search in a high-dimensional robotic hand configuration space: for example, imposing appropriate contact points on the object (e.g. Dai et al., 2013; Lin and Sun, 2013a; Liu et al., 2004; Nguyen, 1988; Ponce and Faverjon, 1995; Roa and Suárez, 2009; Zhu and Wang, 2003). The constraint on contact points, however, is assumed to be independent of physical constraints of a given hand. It raises the problem of solving the inverse kinematics that satisfies the constraints imposed by contact points (Rosales et al., 2011). In this study, we utilized our previous grasp-planning approach presented in Lin and Sun (2014, 2015) to reduce the search space. Here, we provide only a brief description.

To reduce the search space, we integrate human strategy (thumb placement and direction) into grasp planning. We manually indicated the potential thumb placement areas on the object surface with color, shown in the upper left of Figure 8 as an example. Thumb positions offer a general reference of the body part to be gripped, and the workspace of a wrist is highly constrained by the thumb position and direction. As an illustration in Figure 8 we define the Cartesian coordinates of the object, whose x- and z-axes are defined along the horizontal directions of the object, and whose y-axis is defined along the vertical direction, while positive x points left, positive y points up and positive z points to the front. In the upper-left image, several areas on the handle are labeled with different colors to define the learned thumb placements. The color specifies the direction that the thumb tip points to. The side surface of the handle is labeled green, and the top surface of the handle is labeled blue. In the green-colored area, the thumb can point only along $\pm y$ (the up and down directions), while in the blue-colored area the thumb can only point along $\pm z$ (the front and back directions), and so on. During the searching procedure, the program reads in colored

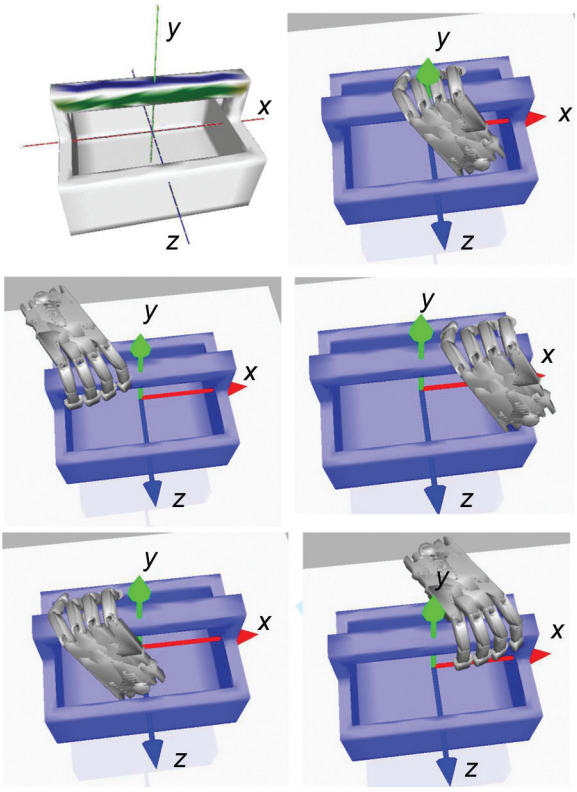

Fig. 8. Illustration of searching procedure constrained by thumb placement and direction. The colored area in the first image is the area where the thumb is allowed to be placed. In this example, we define the Cartesian coordinates of the object as: axes x and z are defined along the horizontal directions of the object, and y is defined along the vertical directions. Further, $+x$ is pointed left, $+y$ is pointed up and $+z$ is pointed towards the front. The top surface of the handle is indicated in blue, and the side surface is indicated in green. Thus, in the green-colored area the thumb can point only to axis y, while in the blue-colored area the thumb can point only to axis z. The examples of grasps during a searching procedure are shown in the images following the upper-left image.

vertices of the object model and moves the thumb by attaching the thumb tip to the colored vertices. The following five sub-figures in Figure 8 show the examples of the feasible grasps found during the searching procedure. For each thumb placement, the wrist position and orientation can be computed from the position and orientation of the thumb tip via forward kinematics. Then, wrist position is dependent on thumb position as well as on the thumb configurations. Using thumb position as a constraint is a practical way to reduce the configuration search space so that the computation of the coverage is feasible.

Once the thumb position is extracted from demonstration, the wrist position and orientation w can be determined via forward kinematics by both the pitch of the thumb relative to the object, and by the thumb joint variables. The workspace of the wrist is highly constrained by the posture of the thumb. Therefore, the objective function becomes

$$Q = f(p, \gamma) \tag{12}$$

where γ is the thumb pitch relative to the object. The search space of the optimization equals $D + 1$, where D is the number of DOFs of the hand joint vector p.

Further dimensionality reduction can be performed on hand DOFs D using some existing approaches. The idea of dimensionality reduction on finger joints was proposed by Santello et al. (1998), who performed principal component analysis (PCA) on the human hand motion data and revealed that the first two eigengrasps (mainly flexion/extension and adduction/abduction) capture more than 80% of the grasp motion variance, implying a substantial simplification of hand postures.

Under the constraint of thumb placement, we are able to use exhaustive search for the optimal grasp. Taking the Barrett hand for example, with the thumb constraint, the search space is reduced to five from ten. Given a thumb placement labeled on the object surface, a number of potential grasps can be generated by changing the pitch of the hand relative to the object and hand-joint angles. The number of grasps to be searched for depends on simulation settings, such as the resolution of the object model, step size of the search space, and the physical robotic hand. An example of power sphere grasp planning by searching through the subspace of relative pitch is illustrated in Figure 9. Instead of exhaustive search, further improvement can be made for the optimization procedure. For detailed discussion, please refer to our previous work (Lin and Sun, 2014, 2015).

3. Results

3.1. Simulation results

In simulation, we tested our approach for several tasks with different objects. The data collection of TWC and grasp planning were programmed with Chai3D and ODE. Non-expert subjects were asked to manipulate an object in the user interface via Phantom OMNI. The interactive

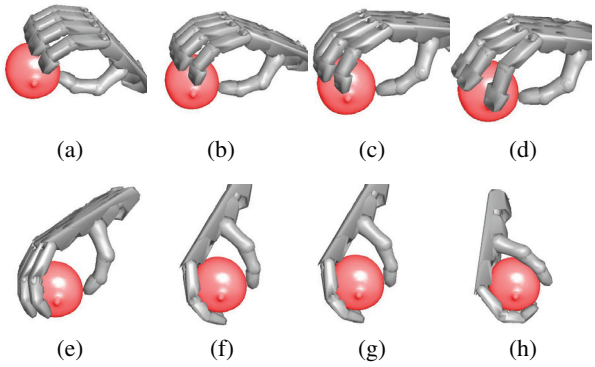

Fig. 9. A procedure of the Shadow hand searching for a power sphere grasp; (d) is a precision sphere grasp, which is rejected because it is not a desired grasp type; (h) is a desired power sphere grasp.

wrenches between the object and the environment were captured during the demonstration with a sample rate of 100 Hz. The data set of the disturbance, compensated for by object gravity, was recorded. Then, from the data set, a non-parametric statistical distribution of the disturbance was built. To reduce the computational complexity, a smaller set of data points was randomly sampled based on the non-parametric statistical distribution.

A Barrett hand model and a Shadow hand model were tested during the simulation for task-oriented grasp planning. Here, we set the friction coefficient μ to be 1. The friction cone is approximated by an eight-sided pyramid. For each hand configuration, contact points and contact normals can be obtained by ODE, and then the GWS can be computed. Grasp quality $Q(G)$ was calculated based on the GWS and the distribution of disturbance. The grasp planning searches for the best grasp configuration that maximizes $Q(G)$.

The value of k is computed according to equation (10): the lower of the values for the task requirement obtained from the TWC and the capability of the robotic hand. The task requirement obtained from the TWC is quantified as the maximum force magnitude of all the data samples in the TWC. The task requirement indicates the amount of force we want the robot to apply. If it exceeds the hand capability, we impose the capability constraint on the contact force.

Figures 10 to 12 show three examples of object manipulation. In the first example, the user was asked to perform a writing motion with a pencil, where the pencil interacts with the environment at the tip. The maximum force magnitude in the TWC is 2.6 N, and the hand capability is 20 N, $k = min(2.6, 20)$, therefore $k = 2.6$. The chosen grasp should be excellent for balancing the pressure and friction on the tip. As shown in Figure 10(a) to (c), task wrenches are biased towards the positive directions of Fy and Fz, rather than the full space of the friction cone. The resulting grasp is, therefore, close to the tip. For the hand configuration shown in Figure 10(d), $Q(G1) = 0.1969$ at $k = 2.6$,

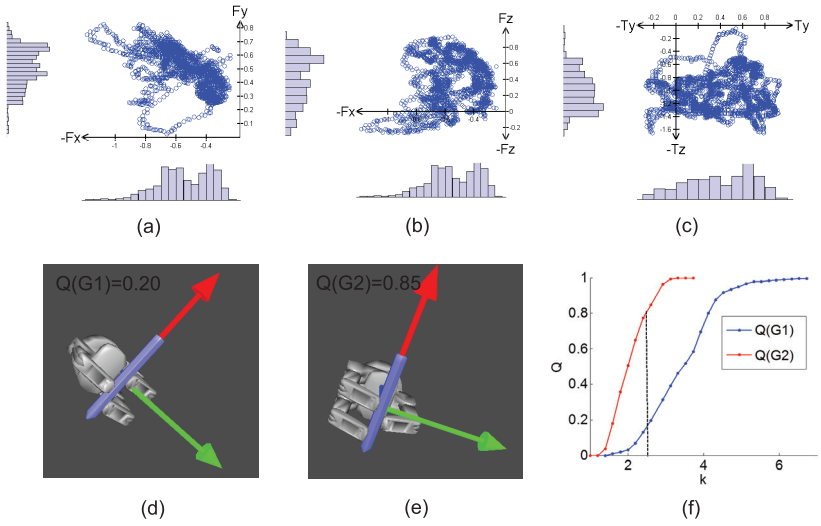

Fig. 10. Planning results for a writing task with a pencil. The center of mass is set to be the origin of the coordinate frame, where axes x, y, and z are indicated in red, green and blue (shown in (d) and (e)). (a) to (c) Distribution of task wrench projected to Fx–Fy, Fx–Fz, Ty–Tz subspaces, respectively, where the task wrench is distributed mainly along the Fx, Fy and Fz directions; torque Tz is small so it is not reported here. (d) and (e) Two different hand configurations; (f) grasp quality Q versus scale k for the two hand configurations shown in (d) and (e).

meaning it covers 19.69% of task wrenches, which is much lower than that of Figure 10(e), where $Q(G2) = 0.8459$ at the same k, because $G2$ is better for applying force along the $+$ Fy and $+$ Fz directions than $G1$ is. The quality measures $Q(G1)$ and $Q(G2)$ changing with scale k for the two grasps are compared in Figure 10(f). The resulting grasp looks different from a human grasp for a writing task, since the proposed grasp quality measure evaluates the grasp only from the perspective of the force requirement, and the hand kinematics is also different from that of human hands.

In the second experiment, grasps were compared for two tasks using a knife. The user was asked to perform a cutting motion along one direction ($+x$ marked in red in Figure 11) and a butter-spreading motion using both sides of the blade. The disturbance distributions for the two tasks are reported in Figure 11(a) to (d). As shown for the cutting task in Figure 11(a), a grasp should be able to generate pressure along the $-z$ direction and friction mainly along the $+$ x direction of the blade. Torque generated along with the force is shown in Figure 11(b). For the butter-spreading task shown in Figure 11(c) and (d), the task wrenches cover a partial area of two opposite friction cones, in other words, the grasp should be able to apply pressure along both $+$ y and $-y$, and friction along $+$ z. The thumb placement is constrained to the handle. Figure 11(e) to (g) contains evaluations of three grasps for the two tasks ($Q1$ for the cutting task and $Q2$ for the butter-spreading task). For the cutting task, the scale k is set to be 8.04 and larger than $k = 3.25$ for the butter-spreading task, selected by the maximum force magnitude in the TWC. It can be seen that for the cutting task the hand configuration in Figure 11(e) is better to apply force in $-Fz$, along with $-Ty$. The hand configuration in Figure 11(g) has the worst-quality measure of the three due to its deficient ability to apply force along the z direction, whereas for the butter-spreading task, the hand configuration in Figure 11(g) is the best and that in Figure 11(e) is the worst.

In the third task, the user was asked to strike a plane with a hammer, and the grasp planning was performed to compare the results of the Barrett hand model and the Shadow hand model. It can be imagined that the chosen grasp should be excellent for balancing large pressure on the head of the hammer. As shown in Figure 12(a) and (b), the distribution covers almost the whole space of the friction cone, whose axis is along the $+$ z direction, and the pressure between the hammer and the environment along the $+$ z direction is as large as 20 N. The designated grasp type during grasp planning is a power grasp in order to perform powerful manipulation. The task requirement exceeds the hand capability, and therefore the scale k of the GWS is set to be the hand capability of 20 for the computation of the quality measure. Figure 12 show the results of searching through the feasible area of thumb placement for the Barrett hand model (Figure 12(c) to (g)) and for the Shadow hand model (Figure 12(h) to (k)). It can be seen that the grasp that is closer to the head is better for counterbalancing the forces that occur at the head. Note that the result for the hammer grasp is different from the intuitive grasping style of humans, who prefer to hold the handle on the other side away from the head, because humans desire to reach a large swing motion with a relatively small arm motion, as well as to generate a large impact force. The grasp optimization considers only the ability to apply

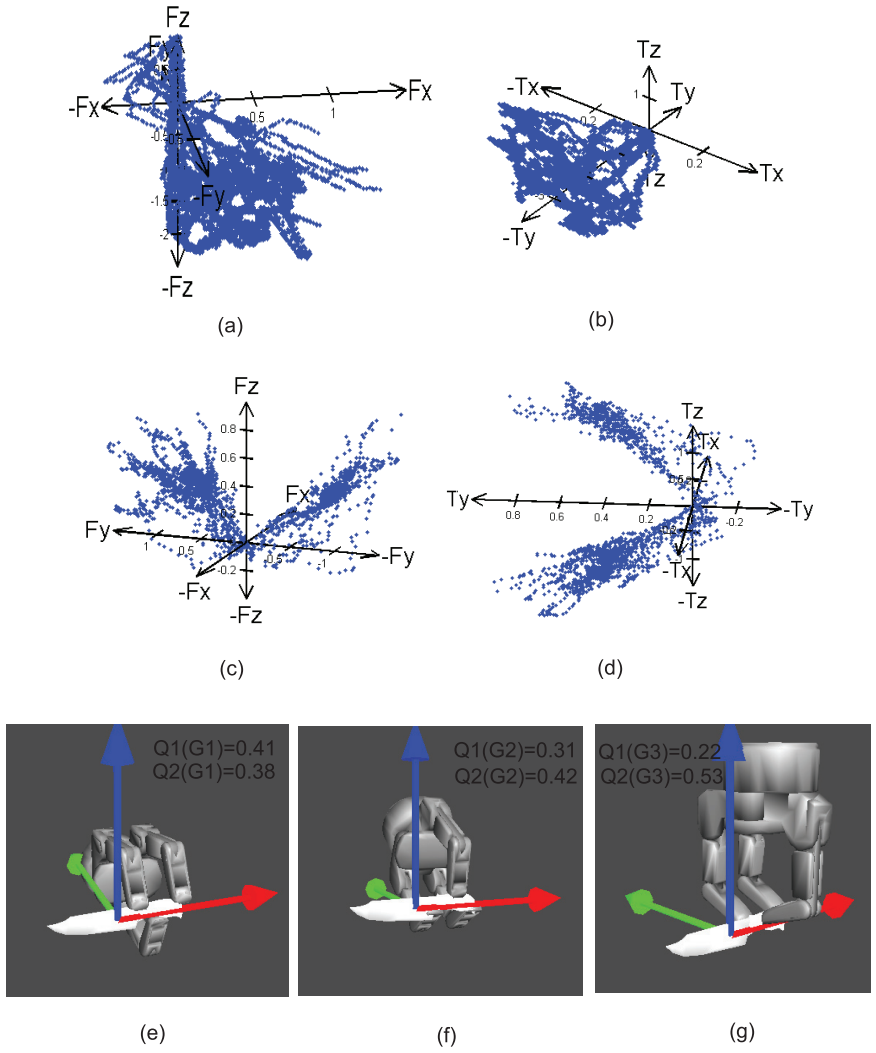

Fig. 11. Planning results for a cutting task and a butter-spreading task with a knife. (a) and (b) Cutting task distribution of task wrenches projected to *Fx–Fy–Fz* and *Tx–Ty–Tz* subspaces, respectively, where the task wrenches are distributed mainly in $-Fz$ and *Fx*. (c) and (d) Corresponding task wrench distribution for butter-spreading task, where the task wrenches are distributed primarily in $+Fy$, $-Fy$, $+Fz$, $+Tz$, $-Tz$. (e) to (g) Three different hand configurations; $Q1$ is the quality measure for the first task, and $Q2$ is the quality measure for the second task. Scale k is set to be 8.04 and 3.25 for the two tasks for precision grasp planning.

finger contact force other than the arm and wrist motions. It can be observed from the figure that similar results were obtained for the two hand models.

As concluded from the experiments, the resulting grasp with a higher grasp-quality criterion tends to be more efficient in applying frequently occurring force, using the same magnitude of resultant force as the low-quality grasp, thus improving the efficiency of power consumption.

3.2. Experimental results on a real platform

Experiments were also performed with a real robot system composed of a Barrett robotic hand and a six-DOF FANUC LR Mate 200iC robotic arm. The Barrett hand is a three-fingered grasper with four degrees of freedom. The system is shown in Figure 13.

In the experiment, objects and manipulation tasks were carefully selected to evaluate the proposed approach. First, because we focused on the success rate of the resulting grasps in executing manipulation tasks rather than simple pick-up tasks, we did not consider tiny objects, such as a pen and a scoop, due to the physical limitation of the Barrett hand in gripping tiny objects precisely. Also, only representative tasks were considered to avoid repetitive tasks. As a result, three representative manipulation tasks were selected to evaluate the proposed approach, including:

- Task 1: move a computer mouse on a table;
- Task 2: plug a power adapter into a power strip;
- Task 3: screw a light bulb into a socket.

Task 1 represents a sliding interaction with the environment. Similar tasks include using a dry-erase eraser,

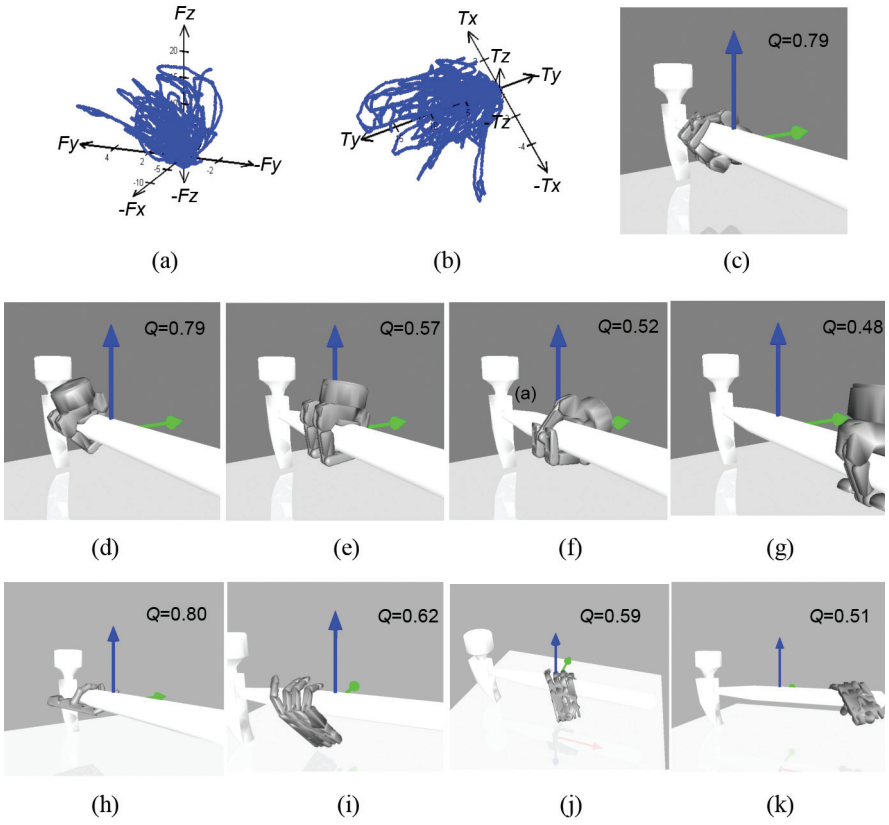

Fig. 12. Planning results for a hammer, where a power grasp is searched for because high power is needed. (a) and (b) Distribution of task wrenches projected to *Fx–Fy–Fz* and *Tx–Ty–Tz* subspaces, respectively, where the task wrenches are distributed mainly in *Fz* and *Ty*. (c) to (g) Five different hand configurations of the Barrett hand model. (h) to (k) Four different hand configurations of the Shadow hand model. Scale *k* is set to be 20.

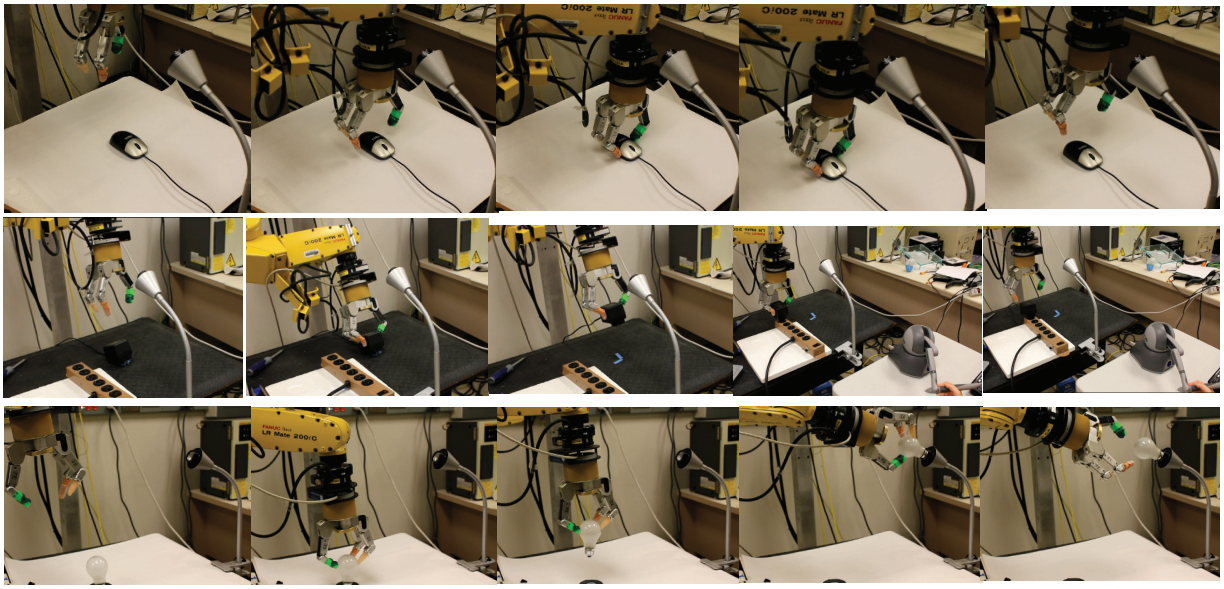

Fig. 13. Snapshots of the robot execution. Top row: the robot approached the mouse, grasped it, and moved it on the table. The whole procedure was done autonomously. Middle row: the robot approached the power adapter, grasped it, and lifted it up autonomously. Then, teleoperation by Phantom OMNI was enabled, and the manipulation task was performed by the user. Bottom row: the bulb was screwed into a socket. The whole procedure setting was similar to the plug manipulation.

moving a broom or a vacuum cleaner on the floor, painting, and so on. Task 2 represents a peg-in-hole motion. Similar tasks include inserting a key or a flash drive, and so on. Task 3 represents a screwing motion. Similar tasks include screwing a screwdriver, jar lid, knob, key, switch, and so on.

Each task was executed in 10 trials. The target object was placed at the same known location and orientation in the robot's workspace for each trial. Before each execution, the robot arm was reset to an initial position, and the robotic hand was kept open. The execution procedure was divided into four steps, as illustrated in Figure 13. The first step was to approach the target object and reach the wrist position and orientation relative to the object which resulted from the algorithm. To avoid potential collision, the robot first moved to 200 mm higher than the target pose, then went straight down until it reached the target pose. Then, the robotic hand was commanded to close its fingers on the object and lift the object up from the table. These first two steps were performed autonomously. The next manipulation step was executed either autonomously or guided by humans, depending on the complexity of the manipulation. The first task, that is, moving a mouse around on a table, was relatively simple, so it was executed in a predefined routine, in which the mouse was moved along a square path on the table. The other two tasks, however, required a complicated sensing and manipulating technique to accomplish the task, which is beyond the focus of this paper. Therefore, we introduced human participation to completing the remaining task by teleoperating the robot using a haptic device, Phantom Omni. After the manipulation step was accomplished, the robot hand was then commanded to open its fingers and move up and away from the object.

The Omni device was chosen due to its compact design and the intuitive positional abilities that we felt would be a good choice for the teleoperation of the robotic arm. The FANUC arm and Barrett hand were connected to the same PC with the Phantom Omni. The manipulator was teleoperated in a position-based and bilateral mode, for which force feedback was provided to the user. The positions and gimbal angles of the OMNI stylus were continuously transmitted to the PC server in real time. The position and orientation of the OMNI stylus were transformed to the corresponding position and orientation of the robot end-effector in its feasible workspace. The robot arm and hand incorporate their own motion controllers. The position commands were streamed from the PC server to the robot controller, so the manipulator was able to follow the OMNI motion in real time. For safety, the speed was constrained up to a feed rate of 30% of the maximum speed. The force sensed by the force sensor embedded in the robot wrist was fed back to the OMNI, so the user was able to feel the contact force when the manipulator was in contact with the environment.

To evaluate the proposed quality measure on a physical robotic platform, we compared the success rate with that of the widely used non-task-oriented planning method that optimizes the epsilon quality ϵ (Ferrari and Canny, 1992). The epsilon quality ϵ measures the radius of the largest six-dimensional ball centered at the origin and enclosed with the convex hull of the UGWS. The epsilon quality refers to the magnitude of the disturbance wrenches that can be compensated for by the grasp in the worst case. The larger the epsilon quality, the more stable the grasp in terms of resisting the worst-case disturbance. We did not compare it to the quality measure k_m discussed above, because it is not trivial to find such an absolute scale of k_m to fit the entire TWS into the GWS without simplifying the shape of the TWS. We did not compare the results with other task-oriented methods either, because to the best of our knowledge none of the related research on task-oriented grasp planning has reported any success rate on the execution of manipulation tasks in a physical system. Most work on real robotic platforms only tested pick-up tasks.

Table 1. Comparison of success rates of proposed approaches using task disturbance with those of the non-task-oriented approach.

Task	Success rate of task-disturbance-based grasp planning	Success rate of non-task-oriented grasp planning
Task 1	60%	40%
Task 2	80%	70%
Task 3	70%	20%
Overall	70%	43.3%

The grasps were being searched for and evaluated by the epsilon quality measure and our proposed quality measure under the same constraints of thumb placement area and grasp types. The resulting hand configurations from both the proposed grasp quality measure and the non-task-oriented grasp quality measure are shown in Figure 14. The first two columns show the optimal grasps resulting from our approach and the epsilon quality measure, with both of the two quality metrics Q and ϵ marked in each corresponding figure. Column 3 and column 4 compare the coverage of the TWC by the two grasps shown in the first two columns. In the figures, the wrench samples in the GWS are marked by blue points, while the wrench samples outside the GWS are marked by red circles. Again, the scale k of the marked quality metric Q was chosen by equation (10). The fifth column shows the proposed task-disturbance-based grasp quality Q as a function of scale k for the two grasps. Since grasps in column 1 are those that maximize our proposed Q and grasps in column 2 are those that maximize ϵ, $Q(G1)$ in column 1 is greater than $Q(G2)$ in column 2, while $\epsilon(G1)$ in column 1 is less than the corresponding value in column 2.

The execution on a real robotic platform of resulting grasps from both the proposed grasp quality measure and the non-task-oriented grasp quality measure for all of the three tasks were compared in Figure 15, and the success rates of the resulting grasps for both quality measures were compared in Table 1. The three examples are also shown in

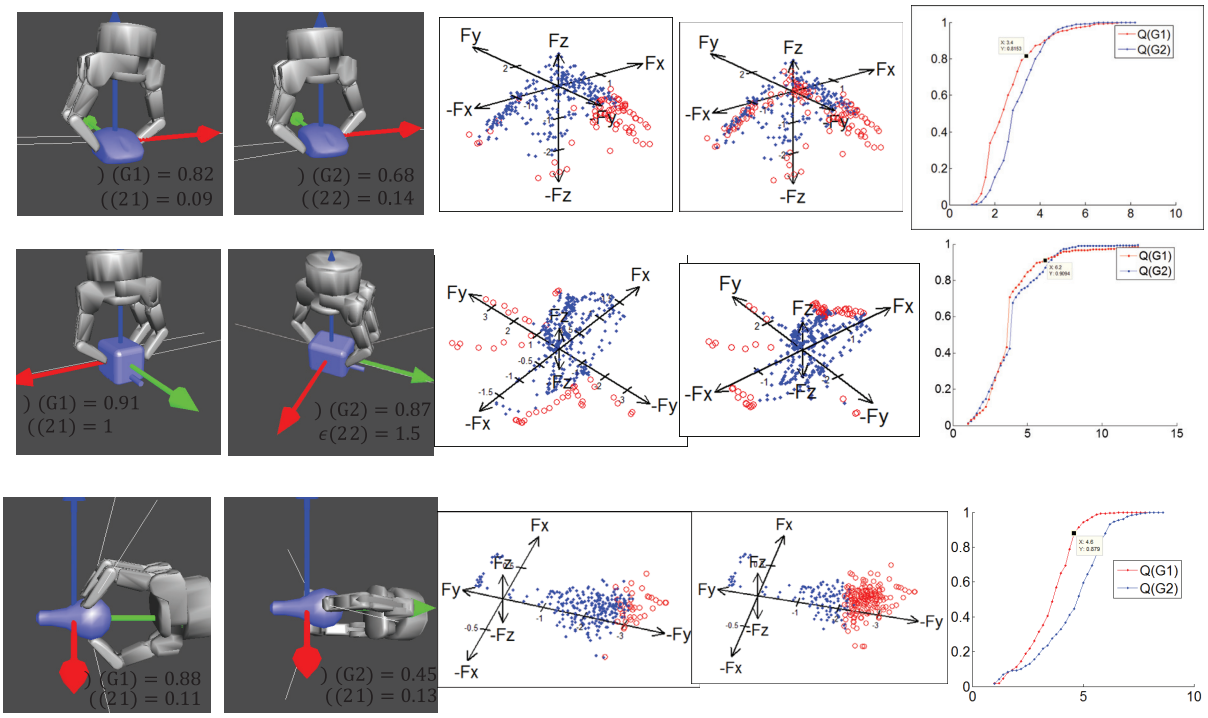

Fig. 14. Simulation results for the selected tasks. The first two columns show the optimal grasps measured by our proposed quality measure Q and by the epsilon quality, respectively. The corresponding quality Q and quality ϵ are marked in each figure. In Task 1, $k = 3.4$; in Task 2, $k = 6.2$; and in Task 3, $k = 4.6$. Columns 3 and 4 compare the coverage of task wrenches by the two grasps shown in the first two columns. Here we only visualized the wrenches in the three-dimensional force subspace. The wrench samples in the GWS are labeled with blue points, while the wrench samples outside the GWS are labeled with red circles. The fifth column shows the proposed quality Q as a function of scale k for the two grasps.

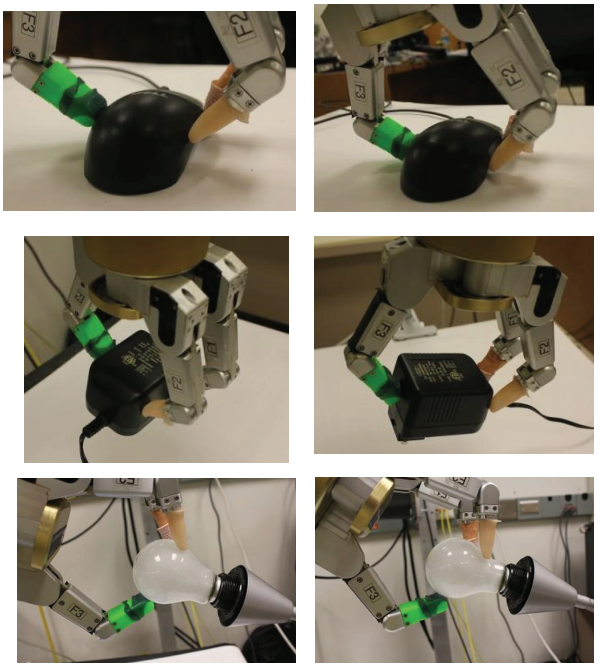

Fig. 15. Evaluation of simulation on the real robotic platform. Left column: execution result from our approach. Right column: execution result from force-closure-based approach.

the supplemental video of Multimedia Extension 1. If the object slid out of the robotic hand during the task execution because of outside disturbance from collision, it was counted as a failure. Otherwise, if the robot successfully completed the task without dropping the object, it was counted as a success. It can be observed that, overall, hand configurations resulting from the proposed quality measure have a higher success rate (average of 70%) compared to that of the non-task-oriented grasp quality measure (average of 43.3%) in executing the manipulation tasks.

The results imply that the proposed quality metric is more consistent with the success rate of the manipulation tasks than the non-task-oriented quality metric.

Task 1 required the robot to slide the mouse on a plane while maintaining contact with the plane. The disturbance was distributed mainly on the boundary of the friction cone (row 1, column 3 in Figure 14), so the grasp was to counteract the friction sliding on the plane and the support force from the plane. Both resulting hand configurations grasped the mouse on the side face (row 1, columns 1 and 2 in Figure 15), but in the latter hand configuration, the fingers were closer to the bottom edge. It was observed in the experiment that in the latter hand configuration the mouse was easier to slide up from the fingers during execution, because the side faces were inclined inward. In Task 2, both

the success rate and the quality Q as a function of scale k are close to each other, although they gripped the object on different faces. The success rates of both approaches appeared to be similar as well. In Task 3, in the latter hand configuration resulting from the non-task-oriented approach, the other two fingers were closer to the base than the thumb. When the robot was trying to screw the bulb into a socket, it was fairly easy for the bulb to be dropped by the robot. In Task 3, the success rate of our approach was much higher than that of the non-task-oriented approach, demonstrating its higher capability to resist the task disturbance.

4. Conclusion

For task-oriented grasp planning, manipulation tasks are known to be difficult to model. In this study, a manipulation task was modeled by building non-parametric statistical distribution of disturbance from demonstration data. Studies on disturbance data indicate that the task wrench is not evenly distributed. Instead, it is possible that disturbance wrenches in some directions occur more frequently than in the other areas, even if they may be smaller than wrenches that occur less frequently. In favor of grasps that are able to apply frequently occurring forces, this paper proposes a task-oriented grasp quality criterion based on the distribution of the task disturbance by computing the ratio of disturbance a grasp covers.

The approach has been validated in simulation with a Barrett hand and a Shadow hand. Both the task model and the demonstration are independent of hand models, so they can be used for other robotic hands. The presented approach was also evaluated with a real robotic system to compare with the non-task-specific automatic grasp planning. Results verify the consistency of the success rate with the proposed disturbance-based quality metric.

There are several limitations to the approach. We modeled the grasp only by contact locations without considering hand configurations. This raises the problem that the contact force may not be applicable by finger joints if they are in "bad" configurations. Some existing works have proposed grasp quality metrics by hand configurations, such as manipulability: the ability of the manipulator to impart arbitrary motions at the end-effector (Yoshikawa, 1985). It can be combined with our proposed quality measure as a global grasp quality measure to give a more complete evaluation of a grasp.

The pen and hammer examples in simulation imply that the resulting robotic grasps may be different from the intuitive grasps of humans, because not only do robots have different hand kinematics than humans, but humans also consider more than the force requirements of a task, for example, motion of the hand and arm to realize the tool actions. Therefore, including both arm and hand motion factors in grasp planning can be a direction of future work. In addition, the TWC can also be updated by the real data collected in robotic manipulation to improve the grasp planning on the fly, given that we cannot guarantee that the TWC during robot execution is always the same as the demonstrated TWS.

Funding

This research received no specific grant from any funding agency in the public, commercial, or not-for-profit sectors.

References

Aleotti J and Caselli S (2010) Interactive teaching of task-oriented robot grasps. *Robotics and Autonomous Systems* 58(5): 539–550.

Barber CB, Dobkin DP and Huhdanpaa HT (1996) The Quickhull algorithm for convex hulls. *ACM Transactions on Mathematical Software* 22(4): 469–483.

Bicchi A and Kumar V (2000) Robotic grasping and contact: A review. In: *IEEE international conference on robotics and automation*, pp. 348–353.

Billard A, Calinon S, Dillmann R, et al. (2008) Robot programming by demonstration. In: Siciliano B and Khatib O (eds) *Handbook of Robotics*. Cambridge, MA: MIT Press.

Borst C, Fischer M and Hirzinger G (2004) Grasp planning: How to choose a suitable task wrench space. In: *IEEE international conference on robotics and automation*, pp. 319–325.

Brock O, Kuffner J and Xiao J (2008) Motion for manipulation tasks. In: Siciliano B and Khatib O (eds) *Springer Handbook of Robotics*. Berlin: Springer.

Dai W, Sun Y and Qian X (2013) Functional analysis of grasping motion. In: *IEEE/RSJ international conference on intelligent robots and systems*.

Ferrari C and Canny J (1992) Planning optimal grasps. In: *IEEE international conference on robotics and automation*, pp. 2290–2295.

Han L, Trinkle JC and Li ZX (2000) Grasp analysis as linear matrix inequality problems. *IEEE Transactions on Robotics and Automation* 16(6): 663–674.

Haschke R, Steil JJ, Steuwer I, et al. (2005) Task-oriented quality measures for dextrous grasping. In: *IEEE international symposium on computational intelligence in robotics and automation*, pp. 689–694.

Hsiao K, Ciocarlie M, Brook P, et al. (2011) Bayesian grasp planning. In: *ICRA workshop on mobile manipulation: Integrating perception and manipulation*.

Hueser M and Zhang J (2008) Visual and contact-free imitation learning of demonstrated grasping skills with adaptive environment modelling. In: *IEEE/RSJ international conference on intelligent robots and systems, WS on grasp and task learning by imitation*.

Kirkpatrick D, Mishra B and Yap CK (1992) Quantitative Steinitz's theorems with applications to multifingered grasping. *Discrete & Computational Geometry* 7(1): 295–318.

Kruger H and van der Stappen AF (2011) Partial closure grasps: Metrics and computation. In: *IEEE international conference on robotics and automation*, pp. 5024–5030.

Kruger H and van der Stappen AF (2013) Independent contact regions for local force closure grasps. In: *IEEE international conference on robotics and automation*, pp. 1588–1594.

Kruger H, Rimon E and van der Stappen AF (2012) Local force closure. In: *IEEE international conference on robotics and automation*, pp. 4176–4182.

Lin Y and Sun Y (2013a) Grasp mapping using locality preserving projections and kNN regression. In: *IEEE international conference on robotics and automation*, pp. 1076–1081.

Lin Y and Sun Y (2013b) Task-oriented grasp planning based on disturbance distribution. In: *International symposium on robotics research*, pp. 1–6.

Lin Y and Sun Y (2014) Grasp planning based on grasp strategy extraction from demonstration. In: *IEEE/RSJ international conference on intelligent robots and systems*, pp. 4458–4463.

Lin Y and Sun Y (2015) Robot grasp planning based on demonstrated grasp strategies. *The International Journal of Robotics Research* 34(1): 26–41.

Lin Y, Ren S, Clevenger M, et al. (2012) Learning grasping force from demonstration. In: *IEEE international conference on robotics and automation*. pp. 1526–1531.

Liu G, Xu J, Wang X, et al. (2004) On quality functions for grasp synthesis, fixture planning, and coordinated manipulation. *IEEE Transactions on Automation Science and Engineering* 1(2): 146–162.

Li Z and Sastry SS (1988) Task-oriented optimal grasping by multifingered robot hands. *IEEE Journal of Robotics and Automation* 4(1): 32–44.

Miller AT, Knoop S, Christensen HI, et al. (2003) Automatic grasp planning using shape primitives. In: *IEEE international conference on robotics and automation*, pp. 1824–1829.

Murray RM, Li Z and Sastry SS (1994) *A Mathematical Introduction to Robotic Manipulation*. Boca Raton, FL: CRC press.

Nguyen VD (1988) Constructing force-closure grasps. *The International Journal of Robotics Research* 7(3): 3–16.

Pollard NS (1994) *Parallel methods for synthesizing whole-hand grasps from generalized prototypes*. PhD Dissertation, Department of Electrical Engineering and Computer Science, Massachusetts Institute of Technology, Cambridge, MA.

Pollard NS (2004) Closure and quality equivalence for efficient synthesis of grasps from examples. *The International Journal of Robotics Research* 23(6): 595–613.

Ponce J and Faverjon B (1995) On computing three-finger force-closure grasps of polygonal objects. *IEEE Transactions on Robotics and Automation* 11(6): 868–881.

Roa MA and Suárez R (2009) Finding locally optimum force-closure grasps. *Robotics and Computer-Integrated Manufacturing* 25(3): 536–544.

Romero J, Kjellström H and Kragic D (2008) Human-to-robot mapping of grasps. In: *IEEE/RSJ international conference on intelligent robots and systems, WS on grasp and task learning by imitation*.

Rosales C, Ros L, Porta JM, et al. (2011) Synthesizing grasp configurations with specified contact regions. *The International Journal of Robotics Research* 30(4): 431–443.

Sahbani A, El-Khoury S and Bidaud P (2012) An overview of 3D object grasp synthesis algorithms. *Robotics and Autonomous Systems* 60(3): 326–336.

Santello M, Flanders M and Soechting J (1998) Postural hand synergies for tool use. *The Journal of Neuroscience* 18(23): 10,105–10,115.

Suárez R, Cornella J and Garzón MR (2006) *Grasp quality measures*. Technical report no. IOC-DT-P 2006–2010. Institut d'Organització i Control de Sistemes Industrials.

Wilk MB and Gnanadesikan R (1968) Probability plotting methods for the analysis for the analysis of data. *Biometrika* 55(1): 1–17.

Yoshikawa T (1985) Manipulability of robotic mechanisms. *The International Journal of Robotics Research* 4(2): 3–9.

Zhu X and Wang J (2003) Synthesis of force-closure grasps on 3-D objects based on the Q distance. *IEEE Transactions on Robotics and Automation* 19(4): 669–679.

Appendix: Index to Multimedia Extension

Archives of IJRR multimedia extensions published prior to 2014 can be found at http://www.ijrr.org; after 2014 all videos are available on the IJRR YouTube channel at http://www.youtube.com/user/ijrrmultimedia.

Table of Multimedia Extension

Extension	Media type	Description
1	Video	Experiments of the three tasks conducted in Section 3.2.